In vivo tumor imaging in mice with near-infrared labeled endostatin

Deborah Citrin,[1] **Andrew K. Lee,**[4] **Tamalee Scott,**[1] **Mary Sproull,**[1] **Cynthia Ménard,**[1] **Philip J. Tofilon,**[3] **and Kevin Camphausen**[1,2]

[1]Imaging and Molecular Therapeutics Section, Radiation Oncology Branch, [2]Vascular Biology Faculty, and [3]Molecular Radiation Therapeutics Branch, National Cancer Institute, Bethesda, MD and [4]Department of Radiation Oncology, University of Texas MD Anderson Cancer Center, Houston, TX

Abstract

Endostatin is a potent inhibitor of angiogenesis currently in phase I clinical trials. Imaging technologies that use near-infrared fluorescent probes are well suited to the laboratory setting. The goal of this study was to determine whether endostatin labeled with a near-infrared probe (Cy5.5) could be detected in an animal and whether it would selectively localize to a tumor. Endostatin was conjugated to Cy5.5 monofunctional dye and injected into mice bearing Lewis lung carcinoma tumors (350 mm²). Mice were imaged at various time points while under sedation using a lightproof box affixed to a fluorescent microscope mounted with a filter in the near-infrared bandwidth consistent with Cy5.5 fluorescence. After i.p. injection, endostatin-Cy5.5 was absorbed producing a near-infrared fluorescent image within the tumors at 18 h reaching a maximum at 42 h after injection. No signal was emitted from mice injected with unlabeled endostatin or Cy5.5 dye alone or those that received no injection. Further results show that a dose response exists with injection of endostatin-Cy5.5. Mimicking the clinical route of administration, an i.v. injection had a peak signal emission at 3 h but also persisted to 72 h. Finally, to determine the intratumoral binding site for endostatin, we performed immunofluorescence on tumor specimens and demonstrated that endostatin binds to tumor vasculature and colocalizes with platelet/endothelial cell adhesion molecule 1 expression. This study demonstrates that endostatin covalently bound to Cy5.5 will migrate from a distant i.p. injection site to a tumor. These data indicate that endostatin-Cy5.5 is appropriate for selectively imaging tumors in uninjured experimental animals. [Mol Cancer Ther. 2004;3(4):481–488]

Introduction

The development of novel cancer treatment strategies is critically dependent on the use of tumors grown in experimental animal models, usually rodents. The inhibition of tumor growth is often an essential parameter in predicting the clinical potential of a given treatment strategy and thus its further development. However, evaluating tumor treatment response typically relies on the gross examination of tumor size through physical examination. This approach severely limits the use of clinically relevant orthotopic tumor models and provides little insight into the tumor processes being affected by the treatment. Clearly, as an indicator of tumor response, the ability to noninvasively image tumor-specific processes or molecules in a laboratory setting would be beneficial in the evaluation of potential antitumor strategies.

Accordingly, angiogenesis would appear to be a well-suited target for the development of such molecular imaging techniques. Angiogenesis is a critical component of tumor growth and survival and has been characterized in terms of several molecular, cellular, and histological parameters (1). Several reports have shown that a small avascular tumor can lie quiescent for years until the angiogenic ''switch'' signals a more permissive environment leading to the in-growth of capillary sprouts (2). The endothelial cells then undergo proliferation, migration, and invasion toward the angiogenic stimulus (3). The labeling index (LI), a marker of cellular proliferation, of stimulated endothelial cells *in vitro* has been reported to be 8.25% (4). Consistent with such *in vitro* results, Denekamp and Hobson showed in an *in vivo* model that the LI of nonstimulated normal tissue endothelium was 0.61% compared with an LI of tumor endothelium of 9.0% (5). This difference between the LIs of normal and tumor endothelial cells suggests that the rapidly proliferating tumor endothelium has the potential to serve as a target for both antivascular and antiangiogenic therapies (6).

Several imaging modalities including ultrasound, computed tomography, magnetic resonance imaging (MRI), and radionuclide imaging such as positron emission tomography (PET) scanning are currently being used to image the tumor microvasculature and the endothelium (7). Nonspecific blood contrast agents for each of these modalities can highlight difference in vascularity between normal and tumor tissues (8, 9). MRI and PET contrast agents can also be engineered to specifically target the vasculature (10). However, major drawbacks in the general application of these modalities in an experimental therapeutic setting include the capital expenditure and technical expertise required to do animal imaging.

With respect to small animal studies, applicable molecular imaging technologies have been developed using three types of substrates: green fluorescent protein (GFP), bioluminescent enzymes (*e.g.*, luciferase), and protease-specific

near-infrared fluorochromes (*e.g.*, Cy5.5; Refs. 11, 12). Utilization of each approach requires that model cells be engineered to express the GFP or luciferase gene, which increases the complexity of imaging intrinsic physiological or pathological process and limits potential clinical application. In contrast, near-infrared fluorochromes can be used to label a variety of targeted molecules eliminating the necessity for engineered cells.

Near-infrared probes in optical imaging offer a variety of benefits when compared with other optical probes such as GFP-based fluorescent probe imaging and bioluminescence imaging. Imaging in the near-infrared spectrum provides increased tissue penetration with minimal tissue autofluorescence (13). Selected near-infrared fluorochromes emit light with tissue penetration approaching 10–15 cm (12), while other optical probes often require surgical exposure of the imaged tissue given the minimal depth penetration of the emitted photons (14). Other benefits of optical imaging include its relatively low cost compared with more traditional imaging systems such as MRI and PET (13, 14).

In the study reported here, Cy5.5-labeled endostatin was used to image *in vivo* murine tumors using a custom-built reflectance imaging system. The results indicate that Cy5.5-labeled endostatin bound strongest to tumor endothelial cells, which allowed for the imaging of tumors in both dose- and time-dependent manner. Moreover, the near-infrared imaging data presented indicate that that endostatin localizes to a site of wound repair.

Materials and Methods

Cell Lines and Cell Culture

A murine Lewis lung carcinoma (LLC-LM) tumor cell line was cultured at 37°C in 5% CO_2 in DMEM with 10% heat-inactivated fetal bovine serum plus 1% glutamine-penicillin-streptomycin as has been described previously (15).

Animals and Tumor Model

Male 4–6-week-old C57BL/6 mice (Frederick Labs, Frederick, MD) were used. Mice were caged in groups of five or less, and their backs and hind limbs were shaved. All animals were fed a diet of animal chow and water *ad libitum*. Animals were anesthetized in an isofluorane chamber prior to all procedures and were observed until fully recovered. Animals were sacrificed by lethal inhalation of carbon monoxide. For the *in vivo* passaging of tumors, animals with tumors ~1000 mm^3 were sacrificed and the skin overlying the tumor was cleaned with betadine and ethanol. A suspension of tumor cells in 0.9% normal saline was made by passing viable tumor through a sieve followed by a series of sequentially smaller hypodermic needles (22–30 gauge) as reported previously (15). Tumor cells (1×10^6) were injected s.c. into the midline dorsum or right hind leg. Tumor diameters were measured with calipers and tumor volumes were calculated using the formula $(L \times W \times W)/2$. All animal studies were conducted in accordance with the principles and procedures outlined in the NIH Guide for the Care and Use of Animals under an approved animal protocol.

Drug Labeling and Injection

Endostatin was labeled with Cy5.5 (Amersham Biosciences, Piscataway, NJ) per manufacturer's instructions. Briefly, 1 mg endostatin in carrier solution was added to a vial of Cy5.5 and mixed thoroughly for 60 min at room temperature. Free Cy5.5 dye was separated from endostatin-Cy5.5 by gel filtration. Molar concentrations of Cy5.5 and endostatin were calculated using extinction coefficients of 250,000 M^{-1} cm^{-1} at 678 nm for Cy5.5 dye and 18 M^{-1} cm^{-1} at 280 nm for endostatin. The molar ratio of Cy5.5 to endostatin was estimated to be 1.0. Endostatin-Cy5.5 was diluted to a final concentration of 1 mg/ml, and 10–100 μl were given as a single i.p. injection or as an i.v. injection. Mice requiring an i.v. injection had central jugular lines placed prior to the tumor implantation. Cy5.5 dye was also prepared in a PBS solution and given as an i.p. or i.v. injection as a control group.

Near-Infrared Detection

Individual mice were anesthetized and restrained in a lightproof box. The reflectance imaging system used a Leica MZFL III fluorescence dissecting scope (Leica Microsystems, Allendale, NJ) with a xenon vapor burner source and an excitation filter system for Cy5.5 (Chroma Technology, Burlington, VT). A custom Cy5.5 filter set was composed of a 625 ± 25 nm excitation filter and a 685 ± 25 nm emission filter compatible with the absorbance and emission maximum of Cy5.5 (675 and 694 nm). Fluorescence was detected using a universal ''C'' mount optical coupler attached to the microscope and a Retiga 1300B camera (Qimaging, Burnaby, BC, Canada) and saved as 16-bit Tiff files using IP Lab (Scanalytics, Fairfax, VA) software processed on a desktop computer. For each imaging procedure, a light image was taken with a typical exposure time of 20 ms immediately followed by near-infrared image capture with a typical exposure time of 6 s. Image processing included segmentation of the tumor on the light image, pasting of this segmented layer over the near-infrared image followed by pseudo-coloring the segment with a relative intensity profile as generated by IP Lab (16). A background measurement, off mouse, upper right of field, was made at each measurement and subtracted from the region of interest relative intensity profile of the tumor.

Immunofluorescence

Histopathological localization of endostatin binding and platelet/endothelial cell adhesion molecule 1 (PECAM-1) expression was performed on tumors, heart, and muscle from untreated animals. Samples were cryopreserved with 30% sucrose, frozen in liquid nitrogen, and sectioned at 6 μm steps. Tissue sections were stored at −80°C until use. For detection of endostatin binding, purified endostatin (NIH Biological Resources Branch Preclinical Repository, Bethesda, MD) was biotinylated and dialyzed to remove unbound product with a Mini-biotin-XX Protein Labeling Kit (Molecular Probes, Eugene, OR). Tissue sections were fixed in acetone at 20°C for 4 min followed by incubation for 30 min in 0.3% H_2O_2 in diluted horse serum. Biotinylated endostatin was applied to sections for 30 min

(1 μg/ml) followed by incubation with Texas Red Avidin D (30 μg/ml; Vector Laboratories, Inc., Burlingame, CA). Avidin/Biotin blocking (Vector Laboratories) was performed per manufacturer's recommendations prior to costaining. To detect PECAM-1 expression, sections were blocked in dilute rabbit serum for 30 min followed by incubation for 30 min with rat anti-mouse PECAM-1 (1:50; PharMingen, San Diego, CA). Sections were then incubated 30 min in biotinylated, mouse-adsorbed rabbit anti-rat IgG (1:200; Vector Laboratories). Fluorescein Avidin D (30 μg/ml) was applied for 30 min followed by counterstaining with 4′,6-diamidino-2-phenylindole. Slides were mounted in Vectashield mounting medium (Vector Laboratories).

Results

To determine whether endostatin bound to the near-infrared fluorochrome Cy5.5 preferentially localizes to tumors *in vivo*, LLC cells were implanted in the right hind leg of C57BL/6 mice and allowed to grow to 500 mm^3 at which point a single i.p. injection of endostatin (20 mg/kg), endostatin-Cy5.5 (20 mg/kg), or Cy5.5 dye alone was given (n = 3/group). Mice were imaged at specified time intervals from 1 to 168 h after injection. Representative images are shown in Fig. 1. Control mice that received no injection were also imaged; tumors in these mice did not fluoresce above background (Fig. 1A). At 18 h, tumors in mice that received no injection, unlabeled endostatin, or Cy5.5 alone emitted no detectable signal (Fig. 1B), whereas in the mice receiving endostatin-Cy5.5, there is a definitive labeling of the tumor (Fig. 1B). The signal intensity detected after the endostatin-Cy5.5 injection increased to reach a maximum at 42 h, which then fades by 114 h (Fig. 1B/D). These results illustrate that there is very little near-infrared background in this system and that endostatin-Cy5.5 localizes to the tumor with a peak signal intensity at 42 h postinjection. Because no signal was detected at 18 h after
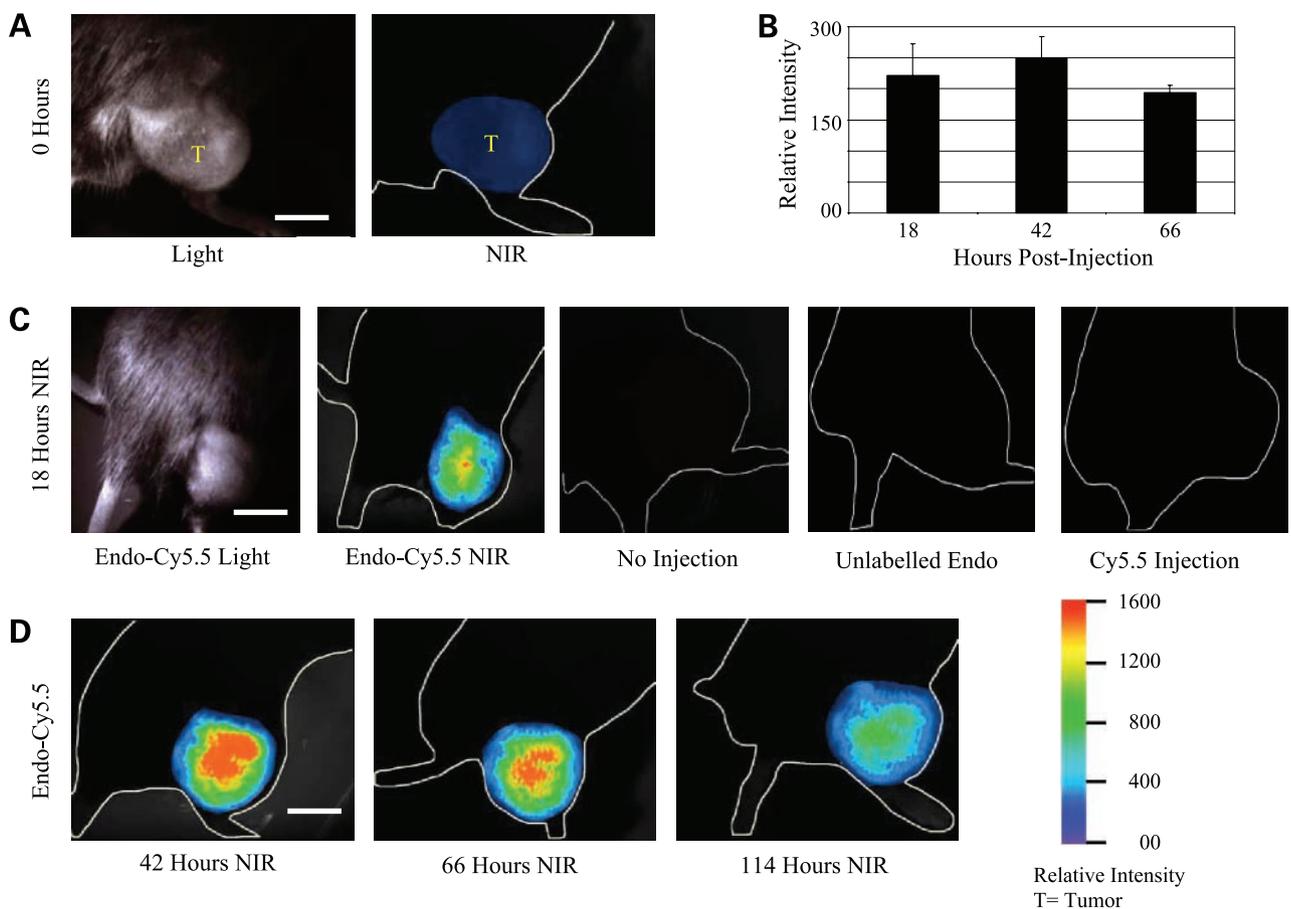

Figure 1. Four representative C57BL/6 mice imaged using a modified lightproof box with custom filter set for near-infrared (*NIR*) mounted into a fluorescent dissecting scope. **A,** images of a mouse implanted with LLC in a previously shorn area that received no injection. There is signal detected only when a filter is not present (*Light*). **B,** quantification of the average relative intensity of the endostatin-Cy5.5 signal at 18 h (n = 6), 42 h (n = 4), and 66 h (n = 3). **C,** near-infrared images of mice that received endostatin-Cy5.5 (*Endo-Cy5.5*), no injection, endostatin alone, or Cy5.5 dye alone at 18 h. **D,** near-infrared signal generated from the C57 mouse that was injected with endostatin-Cy5.5 at 42, 66, and 114 h postinjection. The signal peaks at 42 h but is present at 114 h. A relative intensity profile is to the *right*.
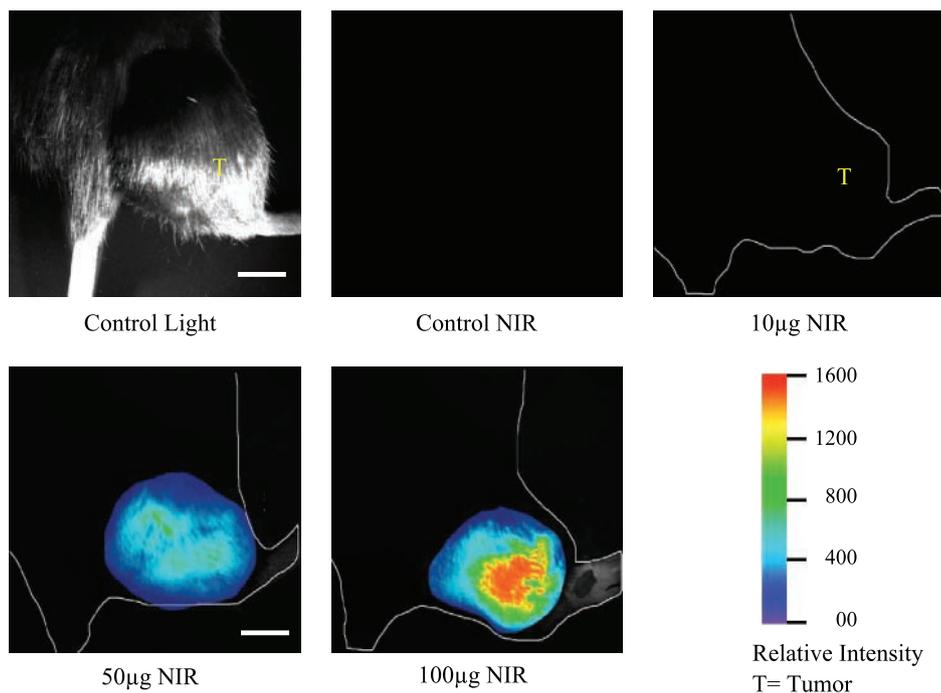
Figure 2. Representative set of images taken from three different unshaven mice injected with 10, 50, and 100 μg endostatin-Cy5.5 and then imaged at 42 h. There is a relationship between dose and signal intensity with 100 μg emitting the greatest signal. A relative intensity scale is to the *right*.

injection of endostatin or Cy5.5 alone, the emission detected in the mice injected with endostatin-Cy5.5 is most likely due to an intact endostatin-Cy5.5 conjugate bound within the tumor.

To determine whether the signal intensity generated within tumors is dose dependent, which would be consistent with the presence of an endostatin receptor, 10, 50, and 100 μg labeled drug were injected i.p. and the mice were imaged at 42 h postinjection, the time point when maximum signal was detected. Figure 2 shows that the image generated is dose dependent with 10 μg producing the least signal, 50 μg producing an intermediate signal, and 100 μg producing the greatest signal.

To further investigate the presence of a putative endostatin receptor, mice were injected with 100, 200, and 500 μg

unlabeled endostatin prior to an injection of 100 μg endostatin-Cy5.5. At 18 h, the relative signal emitted from the mice that received endostatin-Cy5.5 alone compared with the animals that also received unlabeled endostatin was greater (Fig. 3). The dose response shown in Fig. 2 combined with the inhibition of signal emission by unlabeled endostatin is consistent with a putative receptor for endostatin that is binding endostatin-Cy5.5 *in vivo*.

To investigate whether tumor labeling was dependent on the route of administration and to evaluate a more clinically relevant delivery procedure, endostatin-Cy5.5 was given in an i.v. injection. Mice with LLC tumors and central jugular lines received a single bolus of 20 mg/kg endostatin-Cy5.5. As expected, the kinetics of signal onset differed from that observed after i.p. injection. After i.v.
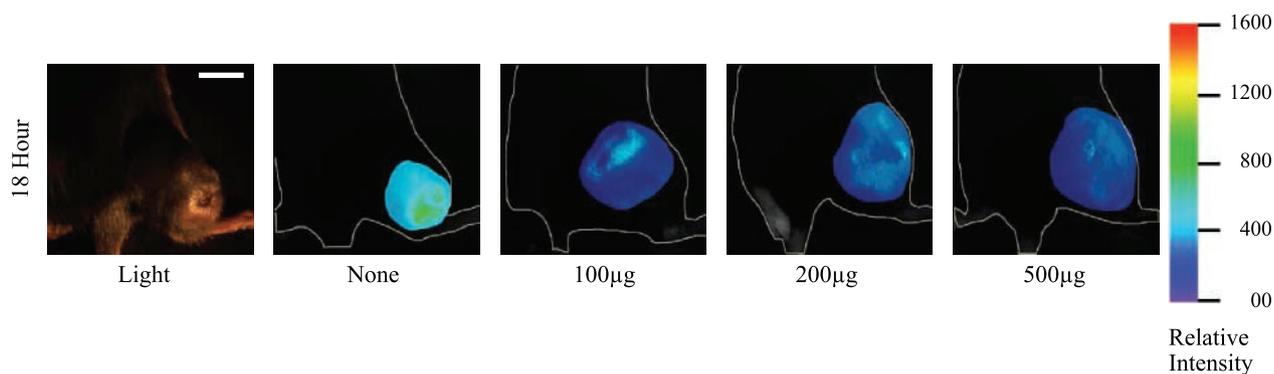

Figure 3. Representative pictures of four mice that received 0, 100, 200, or 500 μg unlabeled endostatin i.p. 30 min prior to an i.p. injection of 100 μg endostatin-Cy5.5. At 18 h, the mouse that received no unlabeled endostatin emitted the greatest signal. The mouse that was injected with 100 μg unlabeled drug had a much weaker signal and the mouse injected with 500 μg unlabeled drug had no signal. This is consistent with a receptor-ligand interaction of endostatin and the tumor endothelium. A relative intensity scale is to the *right*.

injection of endostatin-Cy5.5, maximum tumor intensity was detected at 3 h, whereas the intensity decreased by 24 h and the signal remained detectable out to at least 72 h (Fig. 4). The time course illustrated in Fig. 4 is consistent with other i.v. contrast agents such as radionuclide tracers, which require several hours to saturate the tumor binding sites prior to definitive imaging (10).

To determine whether the endostatin-Cy5.5 specificity for endothelium is tumor specific, we exploited the natural housing conditions of our animals to image a dorsal wound in a mouse. Figure 5 shows the dorsum of a mouse that was injured by his cage mates, injected i.p. with endostatin-Cy5.5 within minutes of the injury, and serially imaged. At 1 h postinjection, there was significant signal in the area of the wound. This persisted out to 42 h at which time granulation tissue was present. These results are consistent with endostatin-Cy5.5 binding to proliferating endothelium in general. However, it should be noted that the kinetics of signal generation were different in tumor *versus* tissue undergoing acute wound healing.

To evaluate endostatin binding in a tumor, immunofluorescence was performed with biotinylated endostatin. A representative micrograph of a tumor section stained with endostatin is shown in Fig. 6. The pattern of staining is consistent with that of the microvasculature with no staining of the tumor cells. A tissue section was dual stained for PECAM-1 (CD31) expression (green), which is specific for endothelial cells, and endostatin binding (red). As shown by the high magnification micrograph in Fig. 6, the endostatin binding coincides with and is limited to areas of PECAM-1 expression on tumor microvasculature. Several areas of the tumor microvasculature do not bind endostatin. There is no detectable binding on tumor cells in Fig. 6. Moreover, endostatin binding was not detected in either skeletal muscle or heart muscle, which served as negative controls (data not shown). The selective staining of tumor microvasculature by endostatin in these frozen tissue sections corresponds with the patterns detected using our *in vivo* imaging approach in Figs. 1–3.

Discussion

Molecular imaging technologies using GFP, luciferase, and near-infrared fluorophores have recently been developed for application in small animal studies. Due to the greater depth of penetration (10–15 cm) and the variety of targeted
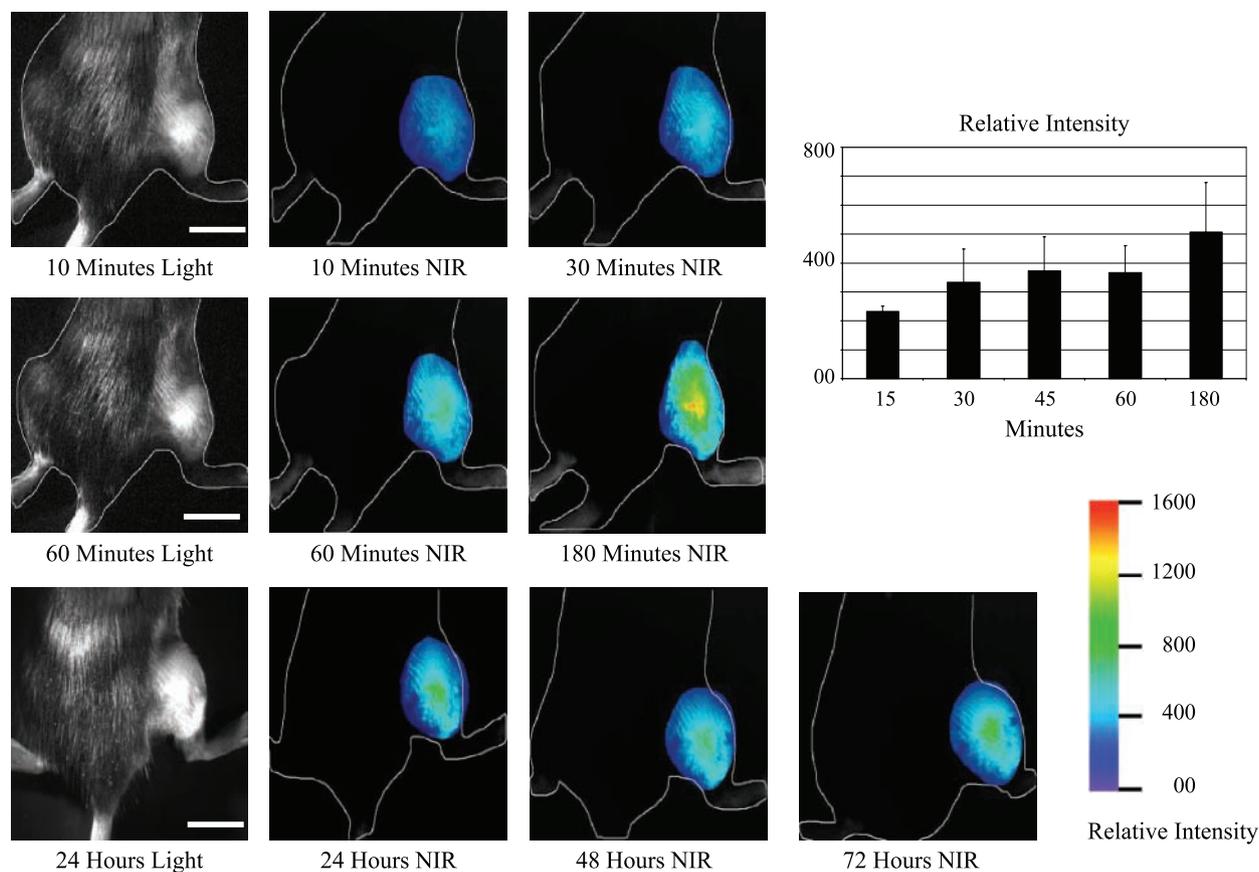

Figure 4. Near-infrared images with pseudocolor overlay of a C57 mouse with a LLC tumor that received an i.v. injection of endostatin-Cy5.5 and was then serially imaged. The peak intensity was different for this group of images with a peak at 3 h that decreased but was present for up to 72 h as seen in the graph to the *right*. The relative intensity curve is also shown to the *right*.

molecules that can be labeled, near-infrared imaging of exogenous molecules targeted to specific processes or sites may provide an imaging approach applicable to experimental therapeutics. Along these lines, Tung *et al.* attached near-infrared fluorochromes to peptides corresponding to the substrate peptide of a tumor-specific enzyme cathepsin D (17). The peptides accumulated in the tumor by extravasation through the permeable microvasculature. A signal is only emitted when the tumor-specific enzyme cleaved the peptide. In a tumor model known to produce cathepsin D, tumors as small as 2 mm were detected *in vivo* using this near-infrared imaging approach (17). This group has expanded their work to include several other enzymes with similar degrees of success (12).

This elegant method to image tumors using a peptide backbone requires an *a priori* knowledge of the enzyme composition of a given tumor. An alternative strategy would be to employ molecules labeled with near-infrared fluorochromes that are specific for a tumor-driven process such as increased proliferation of endothelial cells. This could provide the basis for an *in vivo* imaging system that was independent of tumor type and readily applicable to experimental studies. To pursue such an approach, we labeled endostatin, a protein that has specificity for proliferating endothelial cells (18), with the near-infrared fluorochrome Cy5.5 and imaged its distribution after injection into tumor-bearing and tumor-free mice. The data presented indicate that endostatin-Cy5.5 is specifically incorporated into tumor in a nonwounded animal model in a dose- and time-dependent manner. The time course for maximal signal generation after endostatin-Cy5.5 i.p. injection was of particular interest in that it was not reached until 42 h postinjection. This time frame for maximal signal intensity was not intuitive and would have been difficult to define using an empirical approach.

As antiangiogenic agents are reaching the clinic, the potential for combination therapy with chemotherapy or radiotherapy has been suggested (19). In preclinical models, endostatin and radiotherapy have demonstrated a greater than additive effect on tumor regression (20). Therefore, a noninvasive method for illustrating the kinetics of endostatin accumulation in tumors may allow for defining the optimal timing of endostatin therapy in relation to radiation delivery. The use of a molecular imaging strategy as described here for endostatin should aid in the design of combined antiangiogenic/radiotherapy protocols and may provide insight into the mechanisms responsible for the enhanced tumor control.

Although this near-infrared imaging approach has translational applications in tumor imaging, it also has the potential to contribute to the fundamental understanding of the processes mediating the biological activity of endostatin. For example, whether endostatin exerts its effects through binding to a receptor on proliferating endothelial cells has been the subject of some controversy (21, 22).

Several candidate molecules have been implicated as endostatin receptors including integrin $\alpha_5\beta_1$, glypicans, and KDR/Flk-1 (23–25). The binding of endostatin to specific heparin sulfate domains appears necessary for inhibition of the effects of angiogenic molecules such as vascular endothelial growth factor and fibroblast growth factor 2 (23, 26). Apparently, heparin fragments only as long as 12-mers are required to bind endostatin effectively (26, 27). Karumanchi *et al.* have demonstrated that endostatin binding to heparin sulfate-glycosaminoglycans is necessary for endostatin activity in endothelial cells (23).

The data presented in Fig. 2 showing that endostatin-Cy5.5 locates specifically in tumors in a dose-dependent manner along with the ability of unlabeled endostatin
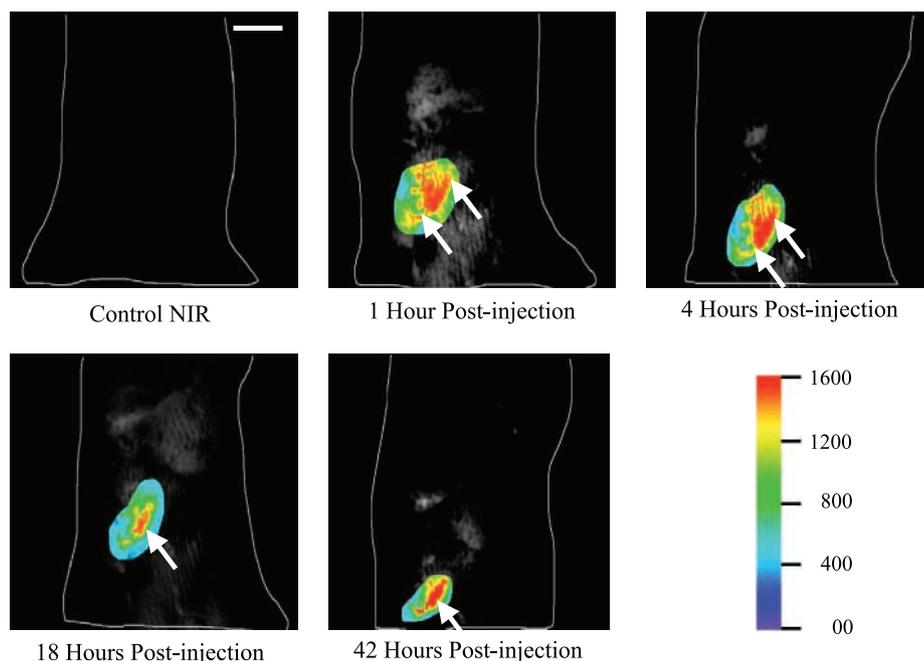

Control NIR   1 Hour Post-injection   4 Hours Post-injection

18 Hours Post-injection   42 Hours Post-injection

Figure 5. Series of picture taken from a mouse that was wounded and given an i.p. injection of endostatin-Cy5.5. There was uptake of drug at 1 h within the wound site that persisted until 42 h when granulation tissue was observed. The relative intensity scale is to the *right*.
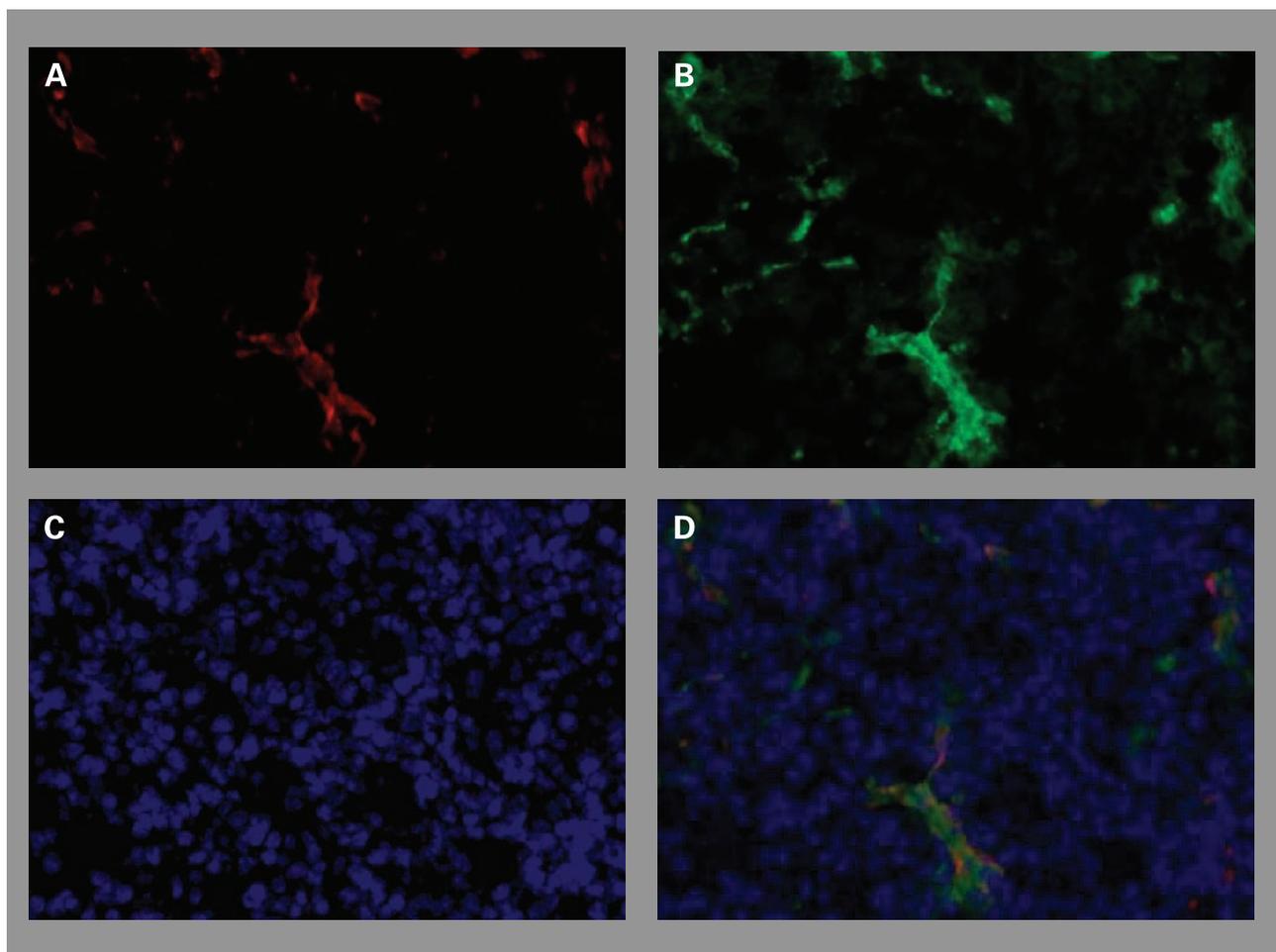
Figure 6. Colocalization of endostatin binding and PECAM-1 expression in tumor sections. **A,** a low magnification image from a tumor stained with biotinylated endostatin. Portions of vessels are stained throughout, while the tumor cells are unstained. **B,** a low power field of the same portion of the tumor stained for PECAM-1. **C,** a low power field of the identical tumor section counterstained with 4′,6-diamidino-2-phenylindole. **D,** an overlay of **A – C** showing the coincidence of endostatin (*red*) and PECAM-1 (*green*). There is overlap of the staining in portions of the tumor vessels.

to prevent the generation of tumor signal (Fig. 3) are consistent with the presence of an endostatin receptor. The histological detection of endostatin binding to the tumor microvasculature (Fig. 6) combined with these imaging results are suggestive of the receptor being located on the endothelial cells within the tumor. Whether endostatin binds only to those endothelial cells in a tumor was addressed in the imaging of a wound in a non-tumor-bearing mouse. Those results clearly showed that endostatin-Cy5.5 localizes to the wound. To our knowledge, this is the first report of an inhibitor of angiogenesis accumulating at a site of wound healing.

Yang *et al.* showed previously that ^{99m}Tc-EC-endostatin selectively binds to tumors in a rat model and concluded that this was consistent with binding to an endostatin receptor (28). The use of ^{99m}Tc-EC-endostatin in a rat tumor model resulted in high signal from multiple organs, including the liver and kidneys, which was confirmed by biodistribution studies. Fluorescence was not detected in

kidney, liver, or other visceral organs or tissues other than the tumor on whole body optical imaging in our model, likely an effect of the depth of these tissues and increased path length required for detection of signal from these organs.

The present study suggests that the near-infrared labeled endostatin can provide translational information, noninvasive tumor imaging, and basic mechanistic information, endostatin receptor binding, in an *in vivo* animal model. As future clinical combination therapy studies are planned, molecular imaging of murine models will become an essential tool in preclinical modeling.

References

1. Folkman J. What is the evidence that tumors are angiogenesis dependant? J Natl Cancer Inst, 1989;82:4 – 6.

2. Fang J, Shing Y, Wiederschain D, et al. Matrix metalloproteinase-2 is required for the switch to the angiogenic phenotype in a tumor model. Proc Natl Acad Sci, 2000;97:3884 – 9.

3. Ausprunk D, Folkman J. Migration and proliferation of endothelial cells in preformed and newly formed blood vessels during tumor angiogenesis. Microvasc Res, 1977;14:53–65.

4. Denekamp J. Endothelial cell proliferation as a novel approach to targeting tumor therapy. Br J Cancer, 1982;45:136–41.

5. Denekamp J, Hobson B. Endothelial-cell proliferation in experimental tumors. Br J Cancer, 1982;46:711–20.

6. Denekamp J. Vascular attack as a therapeutic strategy for cancer. Cancer Metastasis Rev, 1990;9:267–82.

7. Folkman J, Beckner K. Angiogenesis imaging. Acad Radiol, 2000;7:783–5.

8. Cheng W-F, Lee C-N, Chu J-S, et al. Vascularity index as a novel parameter for the *in vivo* assessment of angiogenesis in patients with cervical carcinoma. Cancer, 1999;85:651–7.

9. Miles K. Tumor angiogenesis and its relation to contrast enhancement on computed tomography: a review. Eur J Radiol, 1999;30:198–205.

10. Sipkins D, Cheresh D, Kazemi M, Nevin L, Bednarski M, Li K. Detection of tumor angiogenesis *in vivo* by αV-β3 targeted magnetic resonance imaging. Nat Med, 1998;4:623–6.

11. Hoffman R. Green fluorescent protein imaging of tumor growth, metastasis, and angiogenesis in mouse models. Lancet Oncol, 2002;3:546–56.

12. Mahmood U, Weissleder R. Near-infrared optical imaging of proteases in cancer. Mol Cancer Ther, 2003;2:489–96.

13. Weissleder R, Ntziachristos V. Shedding light onto live molecular targets. Nat Med, 2003;9:123–8.

14. Bremmer C, Ntziachristos V, Weissleder R. Optical-based molecular imaging: contrast agents and potential medical applications. Eur Radiol, 2003;13:231–43.

15. O'Reilly M, Holmgren L, Shing Y, et al. Angiostatin: a novel angiogenesis inhibitor that mediates the suppression of metastases by Lewis lung carcinoma. Cell, 1994;79:315–28.

16. Weissleder R, Tung C, Mahmood U, Bogdanov A. *In vivo* imaging of tumors with protease-activated near-infrared fluorescent probes. Nat Biotechnol, 1999;17:375–8.

17. Tung C-H, Mahmood U, Bredow S, Weissleder R. *In vivo* imaging of proteolytic enzyme activity using a novel molecular reporter. Cancer Res, 2000;60:4953–8.

18. O'Reilly M, Boehm T, Shing Y, et al. Endostatin: an endogenous inhibitor of angiogenesis and tumor growth. Cell, 1997;88:277–85.

19. Camphausen K, Menard C. Angiogenesis inhibitors and radiotherapy of primary tumors. Exp Opin Biol Ther, 2002;2:477–81.

20. Hanna N, Seetharam S, Mauceri H, et al. Antitumor interaction of short-course endostatin and ionizing radiation. Cancer J, 2000;6:287–93.

21. Solaun M, Mendoza L, De Luca M, et al. Endostatin inhibits murine colon carcinoma sinusoidal-type metastases by preferential targeting of hepatic sinusoidal endothelium. Hepatology, 2002;35:1104–16.

22. Strik H, Schluesener H, Seid K, Meyermann R, Deininger M. Localization of endostatin in rat and human gliomas. Cancer, 2001;91:1013–9.

23. Karumanchi S, Jha V, Ramchandran R, et al. Cell surface glypicans are low-affinity endostatin receptors. Mol Cell, 2001;7:811–22.

24. Wickstrom S, Alitalo K, Keski-Oja J. Endostatin associates with integrin and caveolin-1, and activates Src via a tyrosyl phosphatase-dependent pathway in human endothelial cells. Cancer Res, 2002;62:5580–9.

25. Kim Y, Hwang S, Kim Y, et al. Endostatin blocks vascular endothelial growth factor-mediated signaling via direct interaction with KDR/Flk-1. J Biol Chem, 2002;31:27872–9.

26. Kreuger J, Matsumoto T, Vanwildemeersch M, et al. Role of heparan sulfate domain organization in endostatin inhibition of endothelial cell function. EMBO, 2002;21:6303–11.

27. Sasaki T, Larsson H, Kreuger J, et al. Structural basis and potential role of heparin/heparan sulfate binding to the angiogenesis inhibitor endostatin. EMBO, 1999;18:6240–8.

28. Yang D, Kim K, Schechter N, et al. Assessment of antiangiogenic effect using 99m-Tc-EC-endostatin. Cancer Biother Radiopharm, 2002;17:233–46.

In vivo tumor imaging in mice with near-infrared labeled endostatin

Deborah Citrin, Andrew K. Lee, Tamalee Scott, et al.

Updated version	Access the most recent version of this article at: http://mct.aacrjournals.org/content/3/4/481

Cited articles	This article cites 26 articles, 6 of which you can access for free at: http://mct.aacrjournals.org/content/3/4/481.full#ref-list-1
Citing articles	This article has been cited by 4 HighWire-hosted articles. Access the articles at: http://mct.aacrjournals.org/content/3/4/481.full#related-urls

E-mail alerts	Sign up to receive free email-alerts related to this article or journal.
Reprints and Subscriptions	To order reprints of this article or to subscribe to the journal, contact the AACR Publications Department at pubs@aacr.org.
Permissions	To request permission to re-use all or part of this article, use this link http://mct.aacrjournals.org/content/3/4/481. Click on "Request Permissions" which will take you to the Copyright Clearance Center's (CCC) Rightslink site.